Multipath Fading Measurements for Multi-Antenna Backscatter RFID at 5.8 GHz

Joshua D. Griffin[1] and Gregory D. Durgin[2]
School of Electrical and Computer Engineering, Georgia Institute of Technology
777 Atlantic Dr., Atlanta, Georgia 30332–0250
Email[1]: jdgriffin@ieee.org, Email[2]: durgin@ece.gatech.edu

***Abstract*—UHF and microwave backscatter RF-tag systems, including radio frequency identification (RFID) and sensor systems, experience multipath fading that can be more severe than that found in a conventional transmitter-to-receiver channel. Previous work has shown that multipath fading can be reduced on the modulated-backscatter signal received from the RF tag in a non-line-of-sight (NLOS) channel if more than one RF-tag antenna is used to modulate backscatter. This paper presents the first multipath fading measurements for backscatter tags using multiple antennas at 5.79 GHz – the center of the 5.725-5.850 GHz, unlicensed industrial, scientific, and medical (ISM) frequency band that may offer reliable operation for future, miniature RF tags. NLOS measurement results are presented as cumulative density functions (CDF) and fade margins for use in backscatter radio link budget analysis and a detailed description of the custom backscatter testbed used to take the measurements is provided. The measurements show that gains are available for multiple-antenna RF tags and results match well with gains predicted using the analytic fading distributions derived previously.**

I. Introduction

The potential of backscatter radio for use in radio frequency identification (RFID) and sensor applications is great and so are the challenges faced in designing reliable, low-cost backscatter systems with adequate range. At the physical level, the range and reliability of the backscatter radio system is limited by the power consumption of the RF transponder, or RF tag; polarization mismatch losses; object attachment losses resulting from the impedance mismatch and antenna gain reduction caused by the RF tag's close proximity or attachment to dielectric or conductive materials; small-scale fading loss; and losses caused by blockages to the line-of-sight (LOS) between the reader and RF tag. Small-scale fading alone can cause significant reductions in range and reliability and is most pronounced on the modulated-backscatter signal received at the reader. The fading on this signal often follows a product-Rician distribution resulting in deeper fades than those found on the signal received by the RF tag [1].

One way to reduce fading in the backscatter channel is through *antenna diversity* which uses multiple antennas at the reader and RF tag to provide spatially-separated diversity branches. This technique was first explored for backscatter radio by Ingram *et al.* [2] and others [3], [4] have used multiple antennas at the reader for this purpose. Multiple antennas can also be used on the RF tag and it has been shown that modulating backscatter with multiple, spatially-separated RF-tag antennas can reduce small-scale fading on the modulated-backscatter signal [5]. However, no measurement campaigns have been reported that investigate small-scale fading with multiple-antenna RF tags and only a few have studied small-scale fading in the backscatter channel – Kim *et al.* [1] made measurements of the backscatter channel reporting envelope cumulative distribution functions (CDFs) and path loss measurements at 2.4 GHz and Banerjee *et al.* [6], [7] have presented fading measurements as well as spatial and frequency diversity gain measurements at 915 MHz.

This paper presents small-scale fading measurements for RF tags with one and two antennas at 5.79 GHz. This frequency was chosen because it is in the unlicensed, 5.725-5.850 GHz industrial, scientific, and medical (ISM) frequency band available for backscatter radio applications. This frequency band has several potential advantages for backscatter radio systems including reduced antenna size, increased antenna gain, reduced object attachment losses [5], [8] and has been used for at least one passive backscatter radio systems [9]. In the following section, a brief overview of the $M \times L \times N$, dyadic backscatter channel is given followed by a detailed description of the testbed used to take the fading measurements. Afterwards, the measurement procedure and calibration technique are discussed. Finally, the measurement results are presented in terms of envelope CDFs and fade margins for use in backscatter radio link budgets. The measured CDFs are compared to analytic distributions for the $M \times L \times N$, dyadic backscatter channel and a reduction in multipath fading is shown.

II. The $M \times L \times N$ Dyadic Backscatter Channel

Before proceeding, it is useful to briefly outline the $M \times L \times N$, dyadic backscatter channel and the probability density functions (PDF) that describe small-scale fading under non-line-of-sight (NLOS) conditions. The $M \times L \times N$, dyadic backscatter channel is composed of a *forward link* that describes signal propagation from the M reader transmitter antennas to the L RF-tag antennas and a *backscatter link* that describes propagation from the L RF-tag antennas to the N

The work reported in this paper was supported in part by the National Science Foundation (NSF) CAREER Grant #0546955.

J. D. Griffin performed this work while a PhD student at Georgia Tech and is now with Disney Research Pittsburgh, 4615 Forbes Ave., Pittsburgh, PA 15213.

reader receiver antennas. This channel is a *pinhole* channel [10] in which each RF-tag antenna acts as a pinhole through which signals propagate. As more pinholes are added to the channel, fading on the signal received at the n^{th} reader antenna decreases, especially when the forward and backscatter links experience Rayleigh fading. This fading improvement, or *pinhole diversity gain*, arises from the fact that the envelope PDF of the signal received at the n^{th} reader receiver antenna changes shape as the number of RF-tag antennas is increased. The envelope PDF $f_{\mathbf{A}}(\alpha, \rho)$ for the $M \times L \times N$ backscatter channel with Rayleigh-fading forward and backscatter links is given by the following two equations:

$$f_{\mathbf{A}}(\alpha, \rho = 0) = \alpha^{L} \left(\frac{2}{\sqrt{M}\sigma_b\sigma_f} \right)^{1+L} \times \frac{2^{1-L}}{\Gamma(L)} \mathrm{K}_{(1-L)} \left(\frac{2\alpha}{\sqrt{M}\sigma_b\sigma_f} \right), \quad (1)$$

where α is the channel envelope, $\Gamma(\cdot)$ is the gamma function, σ_b and σ_f are the variances of the forward and backscatter links, and $\mathrm{K}_{\nu}(\cdot)$ is a modified bessel function of the second kind with order $\nu = 1 - L$. The second is

$$f_{\mathbf{A}}(\alpha, \rho = 1) = \alpha^{L/2} \left(\frac{1}{\sigma_b\sigma_f\sqrt{M}} \right)^{1+L/2} \times \frac{2^{1-L/2}}{\Gamma\left(\frac{L}{2}\right)} \mathrm{K}_{(1-L/2)} \left(\frac{\alpha}{\sigma_b\sigma_f\sqrt{M}} \right), \quad (2)$$

where $\mathrm{K}_{\nu}(\cdot)$ is a modified bessel function of the second kind with order $\nu = 1 - L/2$ and all other terms are as defined for (1). In these PDFs, ρ denotes *link correlation*, the statistical correlation between the fading on the forward and backscatter links which can extend over the range $-1 \leq \rho \leq 1$. Details of these topics may be found in [5], [11].

III. The Backscatter Testbed

A custom backscatter testbed was designed, prototyped, and used to take the fading measurements reported in this paper. The following sections present the design rationale and overview of the testbed components.

A. Testbed Overview

A simplified block diagram of the bistatic backscatter testbed, which was composed of a combination of laboratory bench and custom equipment, is shown in Fig. 1. The major components of the testbed included an Agilent E8247C signal generator to provide the continuous wave (CW) transmitted signal and local oscillator (LO) for the receivers; two custom, coherent, direct-conversion receivers whose signals were sampled by analog-to-digital conversion boards housed in a personal computer; two custom RF tags whose modulation signal was provided by two Agilent 33250A function generators; custom reader transmitter and receiver antennas; and a screw-drive linear positioner made by Velmex for positioning the RF tags. Further details of the custom-designed equipment is provided below.

1) Reader Antennas: Linearly-polarized patch antennas, shown in Fig. 2, were used at the reader transmitter and receiver. These antennas were designed for 5.79 GHz on an FR4 substrate and each had a broadside gain of approximately 3.8 dBi. Custom antennas were designed because RFID reader antennas for the 5.725-5.850 GHz frequency band are not commonly available.

2) RF Tags: Two RF tags were designed and prototyped for this measurement campaign. The first was a single antenna tag (STAG) and the second was a dual antenna tag (DTAG) whose block diagrams are shown in Fig. 3. The following factors motivated their design:

- **Equal Comparison:** For a fair comparison of fading with the STAG and DTAG, the two RF tags were designed with the same type of antenna and the antennas of the DTAG were made on the same substrate.
- **Flexibility:** The STAG and DTAG designs allowed the backscattered signal to be modulated with an arbitrary bit sequence – i.e. any amplitude shift keying (ASK) waveform. In this realization of the testbed, a differential bit-sequence was output from two Agilent 33250A function generators; however, any source of differential binary signals could be used.
- **Decoupling:** Careful design was required to decouple the closely spaced antennas of the DTAG. This was accomplished using orthogonal DTAG antennas which were each impedance matched to the $50\,\Omega$ switch using Ansoft HFSS, a 3D electromagnetic and microwave software package.

Each RF tag used a 5.79 GHz slot antenna (the DTAG used two such antennas) whose load was switched between an open and short circuit (shorted through a DC block) by a microwave GaAs PHEMT switch (M/A-Com MASW-007107 V2). Each slot antenna was connected to the microwave switch through an ungrounded, coplanar-waveguide (CPW) transmission line, matching section, and DC block as shown in Fig. 4. The switch was toggled using two digital control lines referenced to a third ground line. One potential problem with the STAG and DTAG designs was that the control lines from the signal source could act as an antenna and contribute to the modulated-backscatter signal. To measure the contribution from the control lines, the STAG and DTAG antenna patterns were measured with and without their antennas shorted. When the antennas were shorted with copper tape, the measured pattern was composed of only signals backscattered from the control lines or other unwanted, time-varying scatterers. All of the pattern measurements showed that the backscatter modulated by the control lines was much smaller than that from the un-shorted slot antennas. In general, the desired signal was at least 20 dB greater than that from the control lines and the two only became comparable near the nulls of the un-shorted slot antenna patterns. The STAG and DTAG antenna patterns were dipole-like in shape.

3) Direct-Conversion Receiver: Two custom, direct-conversion receivers, shown in Fig. 5, were designed and prototyped. The receivers downconverted signals from the 5.725-

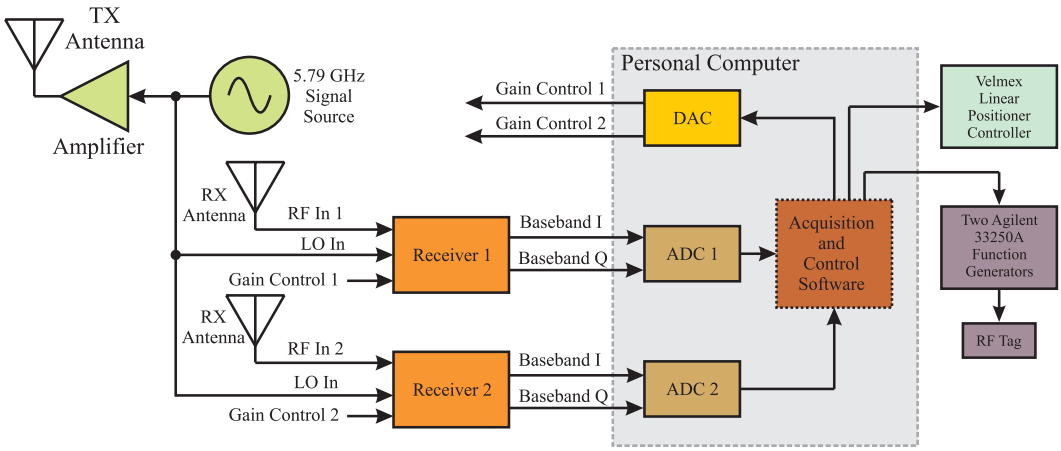

Fig. 1. A simplified block diagram of the backscatter testbed used in this measurement campaign.

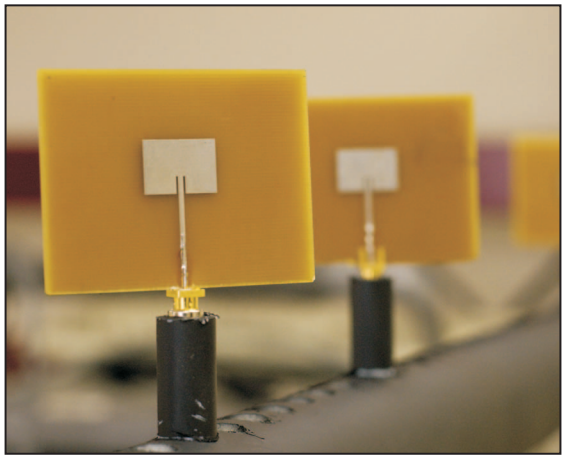

Fig. 2. The 5.79 GHz, linearly-polarized patch antennas used at the testbed transmitter and receiver.

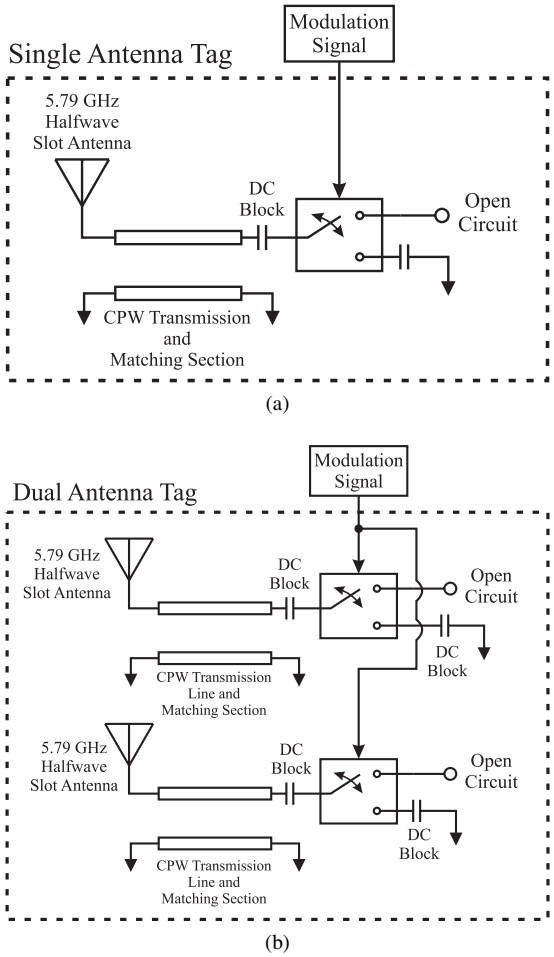

Fig. 3. Block diagrams of the (a) STAG and (b) DTAG.

5.850 GHz ISM band to baseband in-phase (I) and quadrature (Q) signals that were sampled externally. The design of the receivers was motivated by the following:

- **Self-interference Mitigation:** All backscatter radio receivers must be able to receive the strong, unmodulated carrier – i.e. *self interference* – transmitted from the reader while still detecting the much weaker modulated backscatter from the RF tag. These custom receivers were able to receive a -12 dBm self-interference signal while still receiving the small modulated-backscatter signal. The sensitivity and dynamic range of the testbed is discussed in the last paragraph of Section IV. The custom receivers also blocked the self-interference signal after down-converting it to DC which prevented the signal from saturating the baseband amplification stage.
- **Coherent reception:** Coherent reception was required because it is possible for the envelope of the total received signal – i.e. the unmodulated carrier plus the modulated-backscatter signal – to remain constant as the tag switches between its modulation states. Since the phase of the modulated backscatter is not fixed with respect to the phase of the carrier, there are always two possible tag modulation states that will result in the same envelope of the total received signal. In such situations, simple envelope detection would not be able to differentiate between these states.

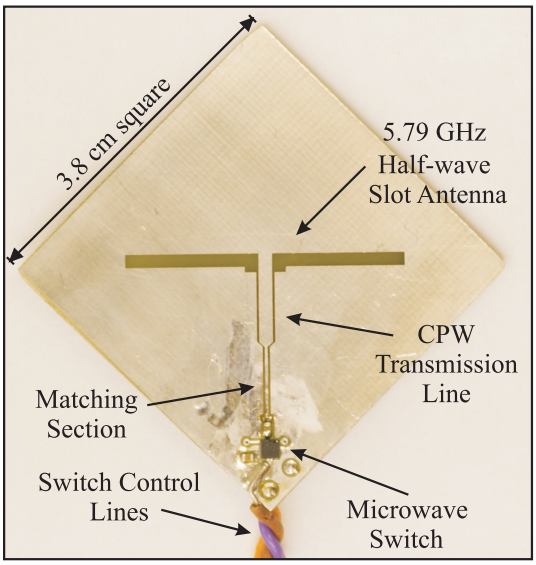

(a)

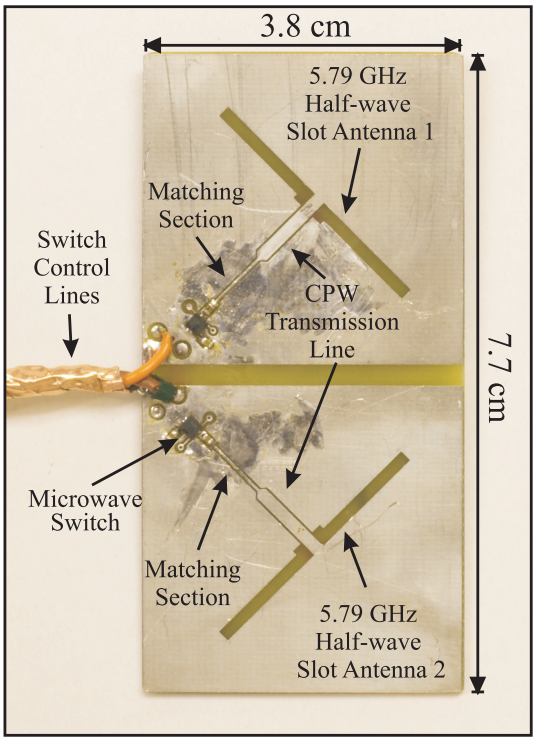

(b)

Fig. 4. The (a) STAG and (b) DTAG showing the 5.79 GHz slot antenna, CPW transmission line, matching section, and microwave microwave switch. The tags were etched on a 62-mil, FR4 substrate.

IV. NLOS Measurement Procedure

The goal of this measurement campaign was to determine the envelope distribution of the $M \times L \times N$, dyadic backscatter channel as a function of RF-tag position at 5.79 GHz ($\lambda_o \approx 5.2$ cm). Fading measurements of two channels are reported:

- **Bistatic $1 \times 1 \times 2$ Channel:** In this channel, the reader transmitter antenna was separated from the two receiver antennas by $6.5\lambda_o$ for RX 1 and $10\lambda_o$ for RX 2. The STAG was used to modulate backscatter.
- **Bistatic $1 \times 2 \times 2$ Channel:** This channel used the same testbed configuration described above, but the DTAG was used to modulate the backscattered signal.

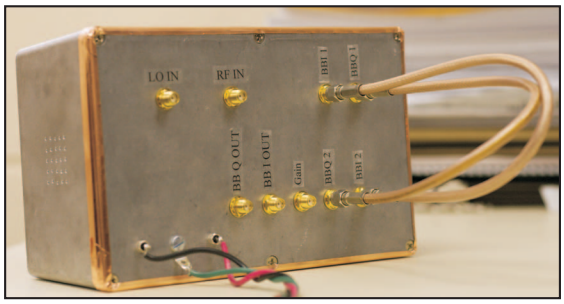

Fig. 5. The custom, coherent, 5.725-5.850 GHz direct-conversion receiver.

These NLOS measurements were "through-wall" – i.e. the backscatter testbed reader was located in room 560 of the Van Leer Building on the Georgia Institute of Technology campus and the RF tag was located in room 558 of the same building as shown in Fig. 6 and Fig. 7. The LOS was blocked by both the sheet-rock wall and a large, metallic sheet (actually, a metallic stripline cavity) for the purpose of creating a rich scattering environment. For each measurement, an unmodulated, 5.79 GHz carrier was transmitted and scattered by the RF tag. The RF tag modulated the backscatter using a 31-bit, maximal-length pseudo-random code (m-sequence) [12] with a chip rate of 1 MHz. The modulated-backscatter signal was received by the two direct-conversion receivers discussed previously and the I and Q baseband signals were digitized and stored for processing. The linear positioner moved the RF tag through a square grid that was 30 cm $\times$ 30 cm (approximately $6\lambda_o \times 6\lambda_o$) and a measurement was taken every 1 cm (approximately every $\lambda_o/5$).

This high spatial sampling rate was necessary because the spatial Nyquist rate for a backscatter channel is twice that of a conventional channel. This is shown in Fig. 8 where the total path length from the reader transmitter to the RF tag and back to the reader receiver $|\vec{r}_f + \vec{r}_b|$ is proportional to $2\,\vec{r}_{tag}$,

$$|\vec{r}_f + \vec{r}_b| = |2\,\vec{r}_{tag} - \vec{r}_{tx} - \vec{r}_{rx}|. \quad (3)$$

Prior to each measurement, the testbed was calibrated by placing the RF tag 40.5 cm from the reader antennas and recording the received signal. The calibration measurements were performed indoors and away from scatterers, were polarization matched, and the tags were close enough to the reader antennas that any multipath signals were not significant. A diagram of the calibration setup for the bistatic testbed is shown in Fig. 9. All STAG and DTAG measurements are reported relative to their respective calibrations.

In these measurements, it was important to ensure that noise did not adversely affect the measured signal, particularly for the small signals measured in a deep fade. If the measured signal was dominated by noise, which can be assumed to

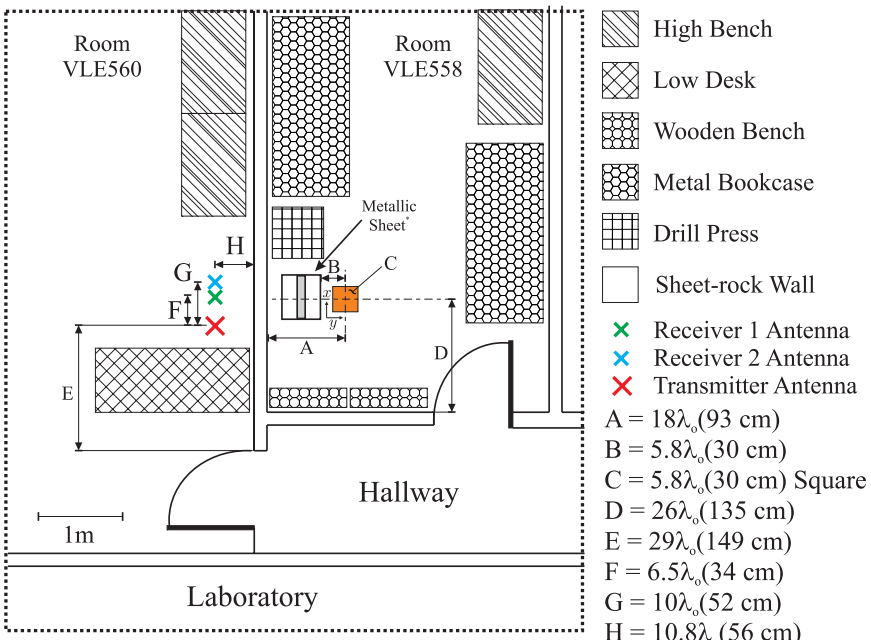

*Note: The base of the metallic sheet (actually a stripline cavity) is 53cm x 46cm. The actual metallic stripline (shown in gray) is 51cm x 10cm x 161cm.

Fig. 6. The bistatic measurement setup between rooms E560 and E558 of the Van Leer Building on the Georgia Institute of Technology main campus. Coherent channel samples were taken at 5.79 GHz as a function of RF-tag position across the orange shaded square. The RF tags were approximately 86 cm above the floor and a channel sample was recorded every 1 cm (approximately every $\lambda_o/5$).

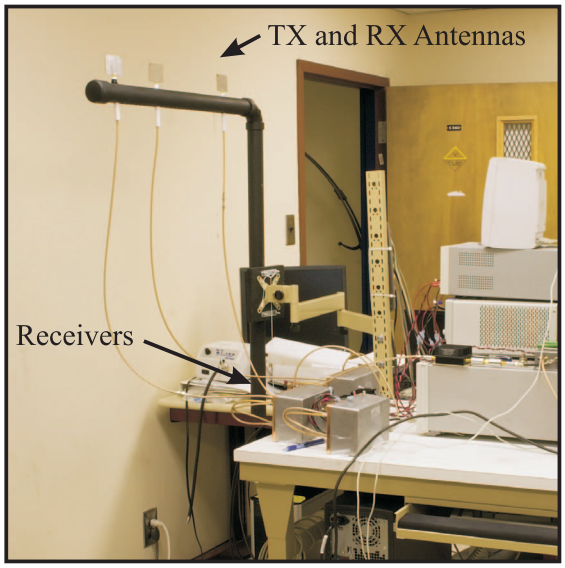

Fig. 7. The testbed setup in room 560 (see Fig. 6) for the through-wall, NLOS measurements. The transmitter and receiver antennas were mounted on a plastic pole and the direct-conversion receivers and signal sources were located on the table. Although shown higher in this photo, the transmitter and receiver antennas were 86 cm above the floor for the measurements.

follow a Gaussian random process, then the resulting envelope distribution would appear to be Rayleigh and hard to distinguish from the expected product-Rayleigh distribution. Therefore, the measured data was compared to the linear-scale mean of the noise power which was measured by operating

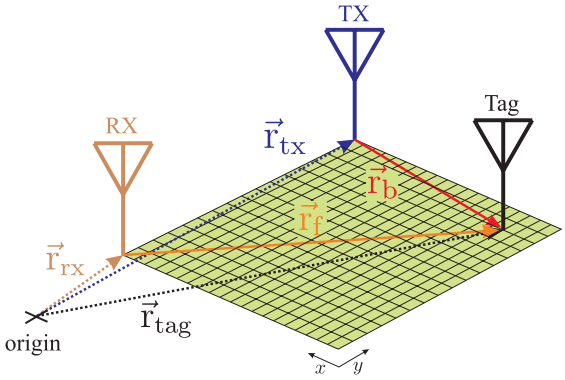

Fig. 8. The relationship between the transmitter-to-tag-to-receiver distance, $|\vec{r}_f + \vec{r}_b|$, and the position of the receiver, transmitter, and RF tag given respectively by $\vec{r}_{rx}$, $\vec{r}_{tx}$, and $\vec{r}_{tag}$. Equation (3) shows that $|\vec{r}_f + \vec{r}_b|$ is proportional to $2\,\vec{r}_{tag}$.

the testbed with no RF-tag modulation. Only measurements that were 20 dB above the linear-scale mean noise power[1] are reported. If the measured envelope is $\alpha_{meas} = \alpha_{true} \pm \alpha_{noise}$, then the percent error caused by noise can be defined as

$$\text{Percent Error} = 100 \times \frac{\alpha_{meas} - \alpha_{true}}{\alpha_{true}}, \qquad (4)$$

where it is assumed that $|\alpha_{true}| > |\alpha_{noise}|$. A 20 dB difference between the noise power and the true signal power results in

[1]The noise power was calculated relative to the STAG and DTAG calibrations.

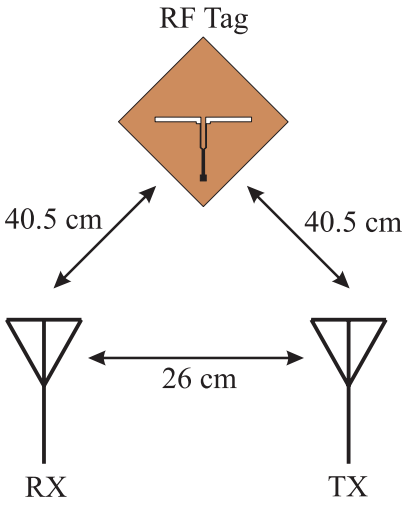

Fig. 9. The calibration setup for the bistatic measurements.

$\pm 10\%$ envelope error. Time averaging was used to lower the noise floor of the testbed and, hence, increase its sensitivity. Thirty-two time averages were used resulting in a noise floor, calculated from the linearly-averaged noise output from the two receivers, of -142 dBm. Since the maximum input power of the receiver is -12 dBm, the useful dynamic range of the testbed is 110 dB.

V. Measurement Results

Backscatter-fading measurement results are presented in terms of envelope cumulative distribution functions (CDF) to explore pinhole diversity gains and fade margins for use in backscatter radio link budgets [8]. The measured CDFs are compared to CDFs calculated from (1) and (2) evaluated for several different channel configurations. As mentioned previously, all of the reported measurements are normalized by the calibration measurements.

A. NLOS Spatial Fading Plots

Before delving into the NLOS envelope distributions, it is useful to examine the channel samples plotted as a function of RF-tag position. Each square in Fig. 10 shows the measured channel power (in dB) for an RF-tag position, relative to the calibration measurements. The power is normalized to the maximum power recorded in each measurement so that the magnitude of each fade can be easily seen. Both the STAG and DTAG plots show deep, rapid fades of up to 40 dB. This high multipath channel consists of waves diffracting around the metallic sheet as well as waves scattered from the drill press, bookcases, and other small clutter not shown in Fig. 6. For reference, the maximum power received in the STAG and DTAG measurements was -82 dBm. Note that this absolute power value is not normalized by the calibration measurements.

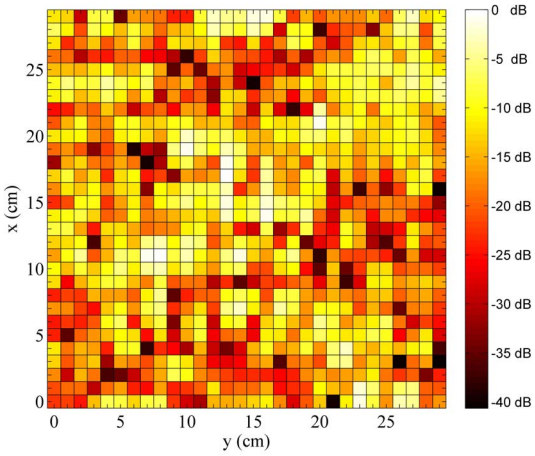

(a)

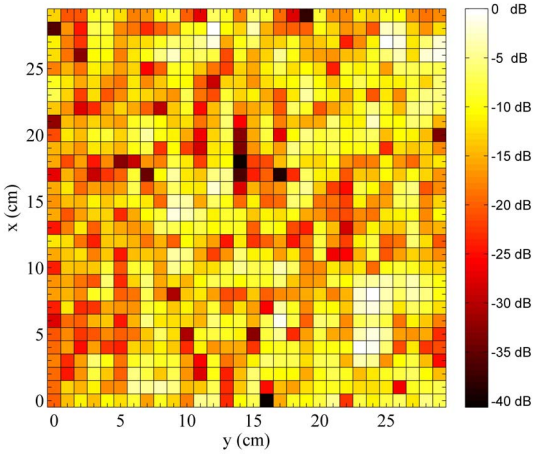

(b)

Fig. 10. The (a) STAG and (b) DTAG measured power in dB relative to the maximum in the NLOS backscatter channel. The orientation of these figures matches that for the measurement diagram shown in Fig. 6. The coloring of each square represents the measured power of the channel at that RF-tag position.

B. Measured Estimates of the NLOS, Backscatter-Channel CDFs

Measured estimates of the NLOS, backscatter-channel envelope distributions for the STAG and DTAG are shown in Fig. 11 along with the corresponding analytic CDFs calculated from (1) and (2).

Visual inspection reveals that the measured estimates of the NLOS CDF match the analytic distributions very well. This observation is confirmed using two error measurements [1]. The first error measurement is the linear mean-square-error (MSE), simply calculated as the average squared difference between the measured and derived CDFs. The second is the logarithmic MSE,

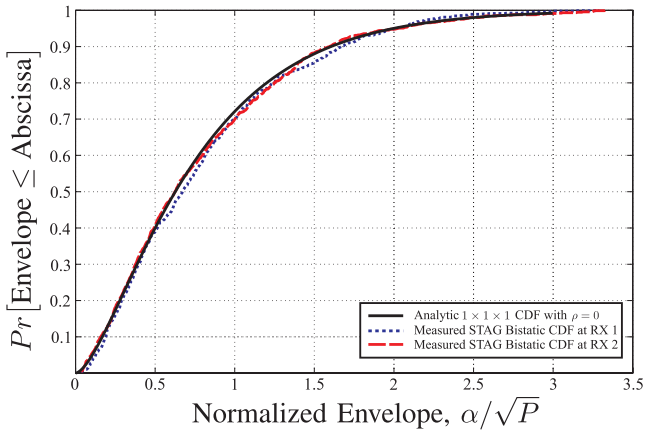

(a)

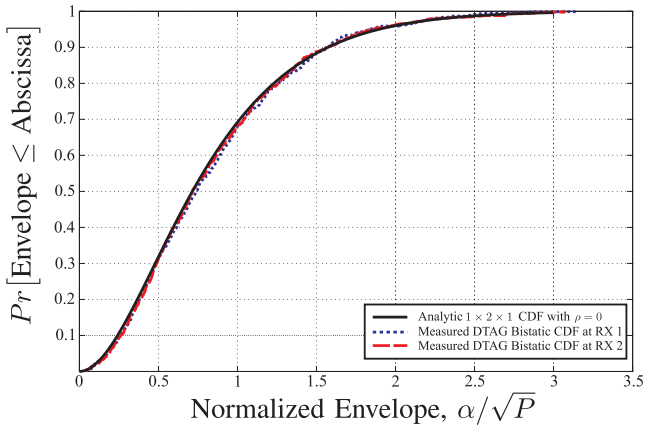

(b)

Fig. 11. The CDF of the bistatic (a) STAG and (b) DTAG measurements in the NLOS backscatter channel along with the corresponding $1 \times 1 \times 1$ and $1 \times 2 \times 1$ CDFs calculated from (1). The CDFs are plotted on axes normalized by the root of the power of each distribution $\sqrt{P}$ for unbiased comparisons.

$$\text{Log MSE} = \frac{1}{N}\sum_{i=1}^{N}\Big[10\log_{10}\big[F_m(\alpha_i/\sqrt{P})\big] - 10\log_{10}\big[F(\alpha_i/\sqrt{P})\big]\Big]^2, \quad (5)$$

where $F_m(\cdot)$ is the measured estimate of the fading CDF, $F(\cdot)$ is the analytical CDF, N is the total number of measured data points, and $\alpha_i/\sqrt{P}$ is the i^{th} measured envelope normalized by the average power of the fading distribution. The average power of the channel distribution is defined as $P = \int_0^\infty \alpha^2 f_{\mathbf{A}}(\alpha)d\alpha$. The logarithmic MSE is useful because it emphasizes the difference between the measured and analytic CDFs for small envelope values – the region of most concern for backscatter radio designers. These error measurements are presented in Table I where the STAG and DTAG measured CDF estimates are compared to the CDFs derived from (1) and (2) for the $1\times1\times1$, $1\times2\times1$, $1\times3\times1$, and $1 \times 4 \times 1$ channels (8 analytic CDFs in all).

For the STAG measurements at RX 1 and RX 2, the analytic $1\times1\times1$ CDF, calculated from (1), minimizes the mean-square error. For the DTAG measurements, the $1 \times 2 \times 1$ CDF from (1) does the same, except that the linear MSE indicates the best match at RX 1 is the $1 \times 3 \times 1$ CDF from (1). In this case, however, since the CDFs for the $1 \times L \times 1$ channels become very similar for large envelopes, the logarithmic MSE is a more meaningful comparison and the best match is likely the $1 \times 2 \times 1$ distribution from (1).

TABLE I
COMPARISON OF THE MEASURED ESTIMATES OF THE CDF FOR THE STAG AND DTAG IN THE NLOS, BISTATIC CHANNEL WITH THE $1 \times 1 \times 1$, $1 \times 2 \times 1$, $1 \times 3 \times 1$, AND $1 \times 4 \times 1$ DERIVED DISTRIBUTIONS FOR $\rho = 0$ (FROM (1)) AND $\rho = 1$ (FROM (2)).

Measured CDF	Linear MSE			Log MSE		
	MMSE	Match		MMSE	Match	
		L	ρ		L	ρ
STAG RX 1	1.57E-4	1	0	9.99E-2	1	0
STAG RX 2	9.85E-5	1	0	1.13E-2	1	0
DTAG RX 1	7.22E-5	3	0	8.92E-2	2	0
DTAG RX 2	4.12E-5	2	0	9.62E-2	2	0

C. Pinhole Diversity in the NLOS Backscatter Channel

Comparison of the measured estimates of the STAG and DTAG CDFs reveals that a pinhole diversity gain exists in this NLOS, bistatic channel, as Fig. 12 shows. The pinhole diversity gain is evidenced by the fact that the STAG CDF is higher than the DTAG CDF for normalized envelope values below approximately 0.8.

Pinhole diversity gains can also be seen by examining the fade margins calculated from the measured CDF estimates. The fade margin is defined as

$$\text{Fade Margin} = 10\log_{10}\left[\frac{\big[F_{\mathbf{A}}^{-1}(\text{Outage Probability})\big]^2}{P}\right] \quad (6)$$

where $F_{\mathbf{A}}(\cdot)$ is the measured CDF estimate and P is the average power of the distribution [8]. The outage probability is the likelihood that the power received at the reader receiver P_{R} has faded below P by an amount equal to the fade margin, Outage Probability $= Pr[P_{\text{R}} \leq P/(\text{Fade Margin})]$ [8]. Table II shows that the fade margin required to maintain a given outage probability is reduced for the DTAG compared to the STAG at each receiver. Furthermore, the fade margins calculated from the measured distribution estimates match those calculated from (1) for the $1 \times 1 \times 1$ and $1 \times 2 \times 1$ channels well.

D. Discussion

The NLOS measured CDF estimates agree well with the $M \times L \times N$ distributions presented in Section II. These measurements show that pinhole diversity gains occur and that (1) is accurate for the $1\times1\times1$ and $1\times2\times1$ channels in bistatic, NLOS channels with rich multipath. The agreement between the derived and measured distribution estimates also indicates that this channel has very small link correlation ρ due to the wide separation between the reader receiver and transmitter

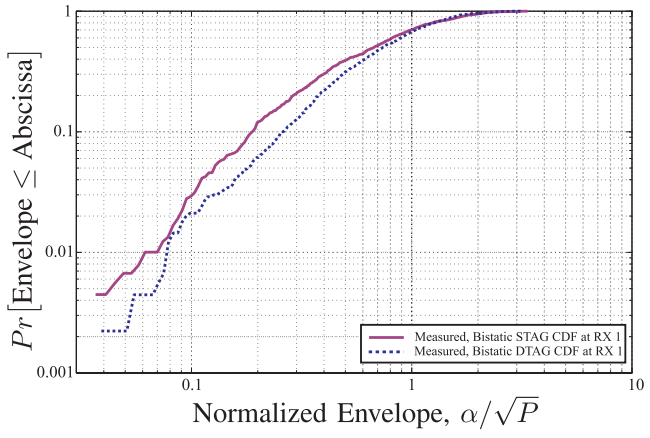

(a)

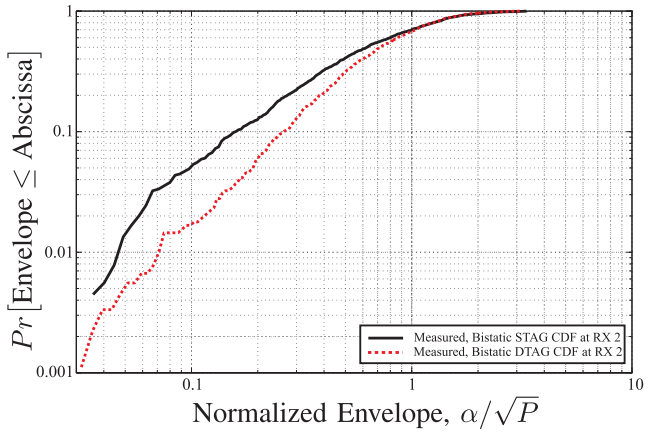

(b)

Fig. 12. The STAG and DTAG CDFs measured at (a) RX 1 and (b) RX 2 plotted on the log-log scale. The CDFs are plotted on axes normalized by the root of the power of each distribution $\sqrt{P}$ for unbiased comparisons.

TABLE II
COMPARISON OF THE FADE MARGINS (IN DB) CALCULATED FROM THE MEASURED CDF ESTIMATES AND THE ANALYTICAL DISTRIBUTION GIVEN BY (1).

Outage Probability	STAG RX 1/2	Eqn. (1) with $L = 1$	DTAG RX 1/2	Eqn. (1) with $L = 2$
0.5	3.4/4.1	4.1	2.6/2.9	2.9
0.1	14/16	15	12/12	12
0.05	18/20	20	15/14	16
0.01	24/27	28	22/23	24
0.005	29/29	32	25/26	26

antennas. The RF-tag antennas are also largely uncorrelated because of the heavy multipath scattering in the channel.

The CDF estimates were calculated from indoor multipath fading measurements; however, they can be applied to any backscatter channel in which the fading follows a product-Rayleigh distribution. In other words, these distributions apply to backscatter channels that do *not* have a dominant specular wave, but are composed of many multipath waves. Product-Rayleigh fading in outdoor backscatter channels may occur less often than in indoor backscatter channels because scatterers may be located farther from the backscatter radio system; however, such a fading distribution is certainly possible in an outdoor environment.

VI. Conclusion

These 5.79 GHz measurements show that fades of up to 40 dB are present on the modulated-backscatter signal received from an RF tag in the NLOS, $M \times L \times N$, dyadic backscatter channel. However, fading can be reduced by modulating backscatter with more than one RF-tag antenna – a pinhole diversity gain. Measurements were presented in terms of CDFs for comparison with previously derived distributions and fade margins for use in backscatter radio link budgets. The measured CDF estimates showed excellent agreement with the analytic distributions derived for the $M \times L \times N$, Rayleigh-fading channel. Likewise, the fade margins were improved by several dB for the DTAG compared to the STAG.

Acknowledgment

The authors would like give a special thanks to Ryan Pirkl for his expert hardware and data processing advice and Joey Duvall for her assistance with the measurements.

References

[1] D. Kim, M. A. Ingram, and W. W. Smith, Jr., "Measurements of Small-scale Fading and Path Loss for Long Range RF Tags," *IEEE Transactions on Antennas and Propagation*, vol. 51, no. 8, pp. 1740–1749, 2003.

[2] M. Ingram, M. Demirkol, and D. Kim, "Transmit Diversity and Spatial Multiplexing for RF Links Using Modulated Backscatter," in *Proceedings of the International Symposium on Signals, Systems, and Electronics*, Tokyo, Japan, July 2001.

[3] J. S. Kim, K. H. Shin, S. M. Park, W. K. Choi, and N. S. Seong, "Polarization and Space Diversity Antenna Using Inverted-F Antennas for RFID Reader Applications," *Antennas and Wireless Propagation Letters*, vol. 5, no. 1, pp. 265–268, 2006.

[4] A. Rahmati, Z. Lin, M. Hiltunen, and R. Jana, "Reliability Techniques for RFID-Based Object Tracking Applications," in *37th Annual IEEE/IFIP International Conference on Dependable Systems and Networks (DSN'07)*, Edinburgh, UK, 2007, pp. 113–118.

[5] J. D. Griffin and G. D. Durgin, "Gains for RF Tags Using Multiple Antennas," *IEEE Transactions on Antennas and Propagation*, vol. 56, no. 2, pp. 563–570, 2008.

[6] S. R. Banerjee, R. Jesme, and R. A. Sainati, "Performance Analysis of Short Range UHF Propagation as Applicable to Passive RFID," in *2007 IEEE International Conference on RFID*, Gaylord Texan Resort, Grapevine, TX, USA, March 2007, pp. 30–36.

[7] ——, "Investigation of Spatial and Frequency Diversity for Long Range UHF RFID," in *IEEE Antennas and Propagation Society International Symposium*, San Diego, CA, USA, July 2008, pp. 1–4.

[8] J. D. Griffin and G. D. Durgin, "Complete Link Budgets for Backscatter Radio and RFID Systems," *IEEE Antennas and Propagation Magazine*, accepted for April, 2009.

[9] B. Strassner and K. Chang, "Passive 5.8-GHz Radio-Frequency Identification Tag for Monitoring Oil Drill Pipe," *IEEE Transactions on Microwave Theory and Techniques*, vol. 51, no. 2, pp. 356–363, Feb. 2003.

[10] D. Chizhik, G. J. Foschini, and R. A. Valenzuela, "Capacities of Multi-Element Transmit and Receive Antennas: Correlations and Keyholes," *Electronics Letters*, vol. 36, no. 13, pp. 1099–1100, 2000.

[11] J. D. Griffin and G. D. Durgin, "Link Envelope Correlation in the Backscatter Channel," *IEEE Communications Letters*, vol. 11, no. 9, pp. 735–737, 2007.

[12] R. W. Dixon, *Spread Spectrum Systems with Commercial Applications*, 3rd ed. New York: Wiley Interscience, 1994.